PHYSICAL REVIEW D **95,** 054512 (2017)

Quark number susceptibilities and equation of state at finite chemical potential in staggered QCD with $N_t = 8$

Saumen Datta,* Rajiv V. Gavai,† and Sourendu Gupta‡

Department of Theoretical Physics, Tata Institute of Fundamental Research, Homi Bhabha Road, Mumbai 400005, India

(Received 1 February 2017; published 31 March 2017)

We report the measurement of quark number susceptibilities (QNS) and their temperature dependence from simulations of QCD with two flavors of light dynamical staggered quarks at finite temperature on 8×32^3 lattices. From the radius of convergence of the Taylor expansion we estimate the critical end point. We use a Padé approximant to resum the series expansion and compute the equation of state at finite chemical potential, namely the baryon number density and its contribution to the pressure. We also report the isothermal compressibility of QCD matter at finite baryon density. Finally we explore the freeze-out conditions for a measure of fluctuations. We examine some sources of systematic and statistical errors in all of these measurements.

DOI: 10.1103/PhysRevD.95.054512

I. INTRODUCTION

Quark number susceptibilities (QNS) [1,2] have become important objects of study in recent years. They are important ingredients in the determination of the phase diagram of QCD [3] as well as the equation of state (EOS) of strongly interacting matter [2,4]. They are also of interest in experimental studies of event-to-event fluctuations of conserved quantities [5–7]. We have earlier presented results with two flavors of light dynamical quarks with lattice spacing of $1/(4T)$ ($N_t = 4$) [3,4] and $1/(6T)$ ($N_t = 6$) [8]. In this paper we push closer to the continuum limit with momentum cutoff of $8T$. Some preliminary results from our current study were discussed in [9,10].

The pressure excess of strongly interacting matter at finite temperature, T, and baryon chemical potential, μ_B, over that at $\mu_B = 0$ is $\Delta P(\mu_B, T)$. We use the Maclaurin series expansion of ΔP in powers of μ_B,

$$\frac{\Delta P(\mu_B, T)}{T^4} = \sum_n \frac{\chi_B^n(T)}{T^{4-n}} \frac{z^n}{n!}, \quad \text{where } z = \frac{\mu_B}{T}, \tag{1}$$

and, due to CP symmetry, the series only has terms in even n, starting from $n = 2$. The coefficients are baryon number susceptibilities (BNS). We shall often use the notation χ_B to mean χ_B^2.

The Maclaurin expansion of Eq. (1) also gives us an expansion for the first derivative, *i.e.*, the baryon number $n(\mu_B, T)$, and the second derivative, *i.e.*, $\chi_B(\mu_B, T)$. At the QCD critical point, $\{\mu_B^E, T^E\}$, there is a critical divergence

$$\frac{\chi_B(\mu_B, T^E)}{(T^E)^2} \propto \frac{1}{|\mu_B^2 - (\mu_B^E)^2|^\psi}, \tag{2}$$

where ψ is a critical index. A Widom scaling argument was used in [4] to show that $\psi = 0.79$ for the Ising universality class, in which the QCD critical point is expected to lie. We have demonstrated earlier that with sufficient statistics one can estimate both $z_E = \mu_B^E/T^E$ [3,4,8] and ψ [4] from lattice determinations of a small number of the baryon number susceptibilities.

More detailed information comes from the QNS. Since we work with two flavors of quarks, there can be two independent chemical potentials, which can be chosen in many ways [11]. One choice is to use them to get number densities of the two flavors of quarks. If we call these μ_u and μ_d, then the QNS are

$$\chi_{\ell m} = \left. \frac{\partial^{\ell+m} P}{\partial \mu_u^\ell \partial \mu_d^m} \right|_{\mu_u = \mu_d = 0}. \tag{3}$$

The order of the susceptibility is $\ell + m$. In our lattice computations the two flavors are degenerate, so $\chi_{\ell m} = \chi_{m\ell}$, and we choose this freedom to set $\ell \geq m$. The BNS are combinations of the QNS. More details can be found in [2], whose notation we follow.

The QNS have been used to test simplified models of QCD, such as Polyakov-Nambu-Jona-Lasinio models [12], effective models based on Schwinger-Dyson resummations of weak-coupling expansions [13], and hadron resonance gas models [14]. They have also been proposed as diagnostics for the presence of composites in the plasma state of QCD [15]. Currently the most interesting use of the BNS is to compare with experiments [6]. All such attempts make the assumption that heavy-ion experiments see signals from thermalized matter whose temperature and

*saumen@theory.tifr.res.in
†gavai@theory.tifr.res.in
‡sgupta@theory.tifr.res.in

TABLE I. The details of the measurements on 8×32^3 lattices. The statistics of gauge field configurations (N) is reported as the number of MD trajectories discarded for thermalization plus the separation between configurations times the number of configurations used. Each MD trajectory was taken to be 6 MD time units long.

β	ma	T/T_c		N	N_v
5.48	0.0144	0.90	(1)	$400 + 10 \times \mathbf{140}$	2000
5.49	0.0139	0.93	(1)	$15000 + 250 \times \mathbf{400}$	2000
5.50	0.0136	0.94	(1)	$15000 + 125 \times \mathbf{737}$	2000
5.51	0.0133	0.96	(1)	$15000 + 250 \times \mathbf{480}$	2000
5.52	0.0129	0.98	(1)	$15000 + 125 \times \mathbf{684}$	2000
5.53	0.0127	1.00		$15000 + 250 \times \mathbf{377}$	2000
5.54	0.0125	1.02	(1)	$15000 + 250 \times \mathbf{375}$	2000
5.60	0.0113	1.14	(1)	$15000 + 250 \times \mathbf{100}$	800
5.77	0.0083	1.53	(2)	$15000 + 250 \times \mathbf{100}$	800
5.96	0.00625	2.07	(4)	$15000 + 250 \times \mathbf{100}$	1600

chemical potentials are then extracted by comparison of experimental data with predictions of equilibrium statistical mechanics. A nontrivial statement about experiments is likely to arise only when such treatments of quite different data are compared. It was pointed out in [5,16] that a comparison of the lattice predictions and experiments can give either a new way of setting the lattice scale [17], or the freeze-out T and μ_B for each collider energy [18].

In the next section we present the details of our simulations, and the necessity of using large fermionic statistics. After that we present results on the QNS and the $\{\mu_B^E, T^E\}$. In the fourth section we report our results on the equation of state, n and ΔP, as well as the isothermal bulk compressibility, κ. In the fifth section we deal with measures of fluctuations and how they relate to experiments. In this section we point out a substantial source of theory systematic errors and suggest how to take care of them. In the final section we summarize our main results and point out certain interesting implications.

II. SIMULATIONS AND STATISTICS

Our simulations were carried out using two flavors of dynamical staggered quarks with $m_\pi/m_\rho \simeq 0.4$ and $N_t = 8$ (see Table I for details of the runs). It has been known for long that $N_f = 2$ QCD at finite quark mass has no phase transition [19]. In [20] it was shown that there is no privileged operator which measures a crossover temperature. In fact, a follow-up study [21] showed that the crossover in QCD with physical quark masses is so broad that different measures of the crossover temperature built using the renormalized chiral condensate alone gave results which could differ by more than 7% of their mean. This is about 5–6 times the error bar on each. The difference between the crossover temperature determined using the Wilson line and the chiral condensate is less than 3 times the error bar. The lesson for subsequent lattice studies is that it is sufficient to use the simplest of measures of the crossover, unless the goal is to improve the precision of the temperature scale. We have used the Wilson line susceptibility, as we had in earlier studies. As a result, our temperature scales and other results are directly comparable to our older results on coarser lattice spacings.

A previous study with staggered quarks on $N_t = 8$ lattices [22] used the chiral condensate and the Polyakov loop, L, to locate a crossover coupling in the range $5.52 \le \beta \le 5.56$. We had earlier set the scale for a study with coarser lattices ($N_t = 6$) using the maximum of the Polyakov loop susceptibility, χ_L. Two-loop scaling using a nonperturbative value of the gauge coupling [8] indicated that the crossover measured by χ_L would lie close to $\beta = 5.54$. In our direct computation we found that the crossover occurs at $\beta = 5.53$. Such a shift corresponds to an uncertainty in the temperature scale of about a percent and is expected when using two-loop scaling with these cutoffs [23]. Using the new, finer, lattice cutoff, we set the relative temperature scale as before. The systematic errors in scale setting are estimated by comparing computations in different renormalization schemes. We found that this error is about 1%.

Numerical computation of operators with multiple fermion loops is time consuming. Fast and accurate computations of the trace of a large and sparse matrix, A, involves a noisy estimator: $2\mathrm{Tr}A = \overline{r^\dagger A r}$ where r is a complex vector drawn randomly from an appropriate ensemble (here, Gaussian), over which we average. Every fermion loop is such a trace over the lattice discretized Dirac operator. To get high accuracy in products of traces, we need a large number, N_v, of random fermion source vectors. Since the evaluation of thermal expectation values of traces involves a Monte Carlo simulation (over fermion sources) within a Monte Carlo simulation (over gauge configurations), we use a bootstrap over both in order to estimate means and errors.

To stabilize measurements of the QNS, we require successively larger N_v as the order increases. This is largely due to the increasing number of fermion-line disconnected loops which can contribute as the order increases. This can be seen even at the lowest nontrivial order, *i.e.*, for χ_{20}. Below T_c, the operator $\mathcal{O}_{11}$ (see [3] for a definition of these operators) contributes around 15% of the mean value, but about 50% of the error. The situation is much worse at $2T_c$ where this operator contributes about 0.2% of the mean, but about 33% of the error. Fermion-line disconnected operators, $\mathcal{O}_{n_1 n_2 n_3 \cdots}$, are the main source of noise since they turn out to be fat-tailed [4]. At present there is no better way of controlling them than by increasing N_v.

In Fig. 1 we show that at low temperatures a reasonable estimate of χ_B^n for $n = 6$ requires N_v as large as 1000. The number of gauge configurations used is also important, and we have used a minimum of around 400 gauge configurations at low temperatures in order to get about 20% errors for $n = 6$. As one sees from the data shown in the figure, such statistics are essential.

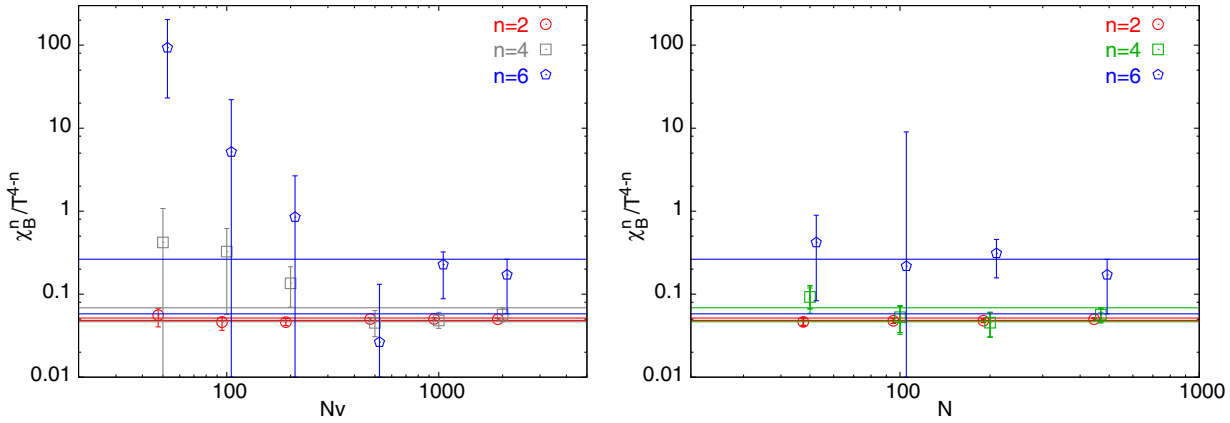

FIG. 1. The series coefficients of χ_{20} computed at $T/T_c = 0.94(1)$, shown as functions of the number of fermion source vectors, N_v, (first panel) and the number of gauge configurations, N, (second panel) used. Note that χ^4 is displaced slightly to the right in order to alleviate clutter.

At high temperature the problem simplifies a little. In Fig. 2 we show how the estimates for the QNS depend on N_v at $2T_c$. In the high temperature phase we see that $N_v \simeq 400$ is enough to control errors. Configurations are also smoother at high temperature, so the number of gauge configurations required is also smaller. $N_v \simeq 400$ also begins to control the approach to an accurate measurement of eighth order susceptibilities. Of these the diagonal susceptibility $\chi_{80}T^4$ has the largest errors; we can trace this to fluctuations in a single noisy operator, $\mathcal{O}_{2222}$. Since the higher order QNS are divided by large factorials in Taylor expansions, this degree of control over errors suffices for extrapolations to finite chemical potential. The figure also demonstrates that the off diagonal QNS are in pretty good agreement with weak coupling computations at $2T_c$.

III. SUSCEPTIBILITIES AND THE CRITICAL POINT

In Fig. 3 we show the second order QNS as functions of T/T_c for different lattice spacings. The measurements with lattice spacing $1/(4T)$ were presented in [3] and recently updated in [4]. The data shown in Fig. 3 for this cutoff comes from [4]. For lattice spacing of $1/(6T)$ we use the data of [8]. Two regions of temperature are clearly visible, that above and below T_c. Below T_c the data on χ_{11}/T^2 from lattices with cutoff of $6T$ are seen to be more noisy. This reflects the fact that these older measurements used significantly smaller number of gauge configurations. Below T_c the diagonal QNS, χ_{20}/T^2, changes little when the lattice cutoff is changed from $6T$ to $8T$. This is shown more clearly in the zoom presented in the second panel. This indicates that finite lattice spacing effects are small in χ_{20}/T^2 for $T < T_c$ when going from $N_t = 6$ to 8.

When the system is heated above T_c, χ_{11}/T^2 is very close to zero in the weak-coupling expansion, and that is also seen in this figure for $T > T_c$. However, χ_{20}/T^2 is seen to have a strong dependence on the lattice spacing in this region of T. The difference in the behavior of the two second order QNS at high temperature is due to an interesting phenomenon. There is an operator, $\mathcal{O}_2$, which contributes to χ_{20}/T^2 but not to χ_{11}/T^2. This operator has a nonzero value for free fermions, but is subject to a large finite lattice spacing effect. Weak-coupling corrections to

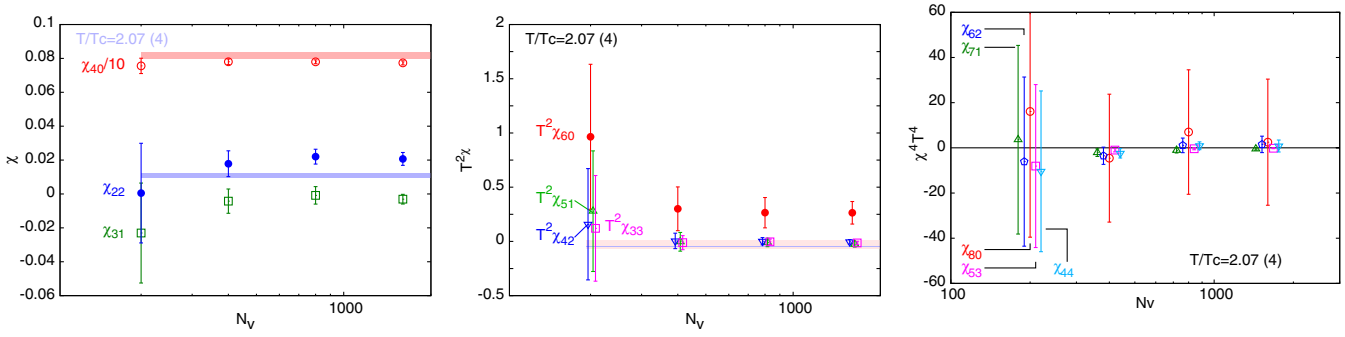

FIG. 2. The fourth order (first panel), sixth order (second panel) and the eighth order (third panel) QNS at $2T_c$ as functions of the number of fermion source vectors, N_v, used. Different QNS for the same order have been displaced from each other for visibility. χ_{40} has been scaled down by a factor of 10 in order to fit into the scale shown. In the first panel the pink band is a weak coupling prediction for χ_{40} and the blue band for χ_{22} [24]. In the second panel the pink band is a weak coupling prediction for χ_{60} and the blue band for χ_{42} [24].

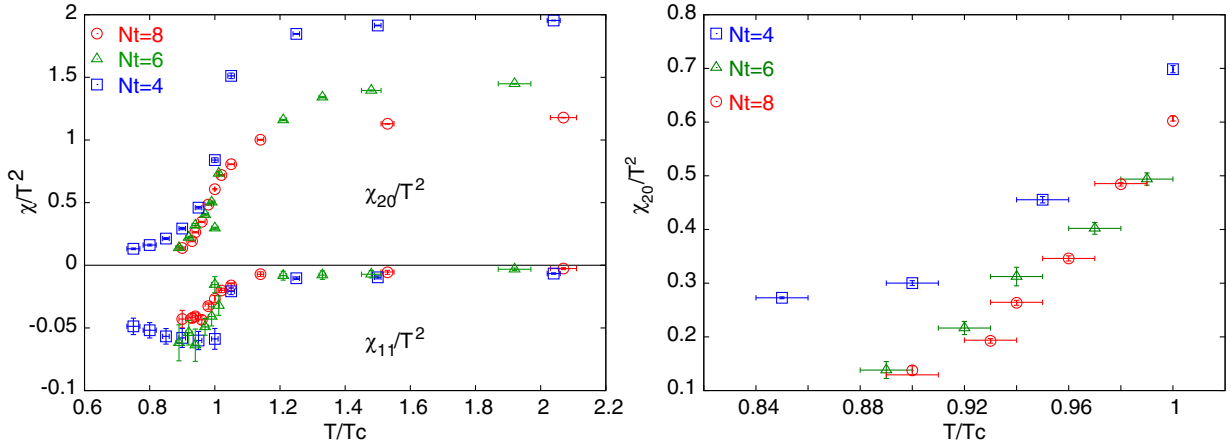

FIG. 3. The first panel compares χ_{20}/T^2 and χ_{11}/T^2 as a function of T/T_c with different lattice cutoffs $a = 1/(TN_t)$. Notice the difference in scale for the two quantities. In the second panel we zoom into the region of $T < T_c$, for χ_{20}/T^2, since it is relevant to the position of the critical point, as we discuss later.

this operator are small. As a result, this QNS shows strong finite lattice spacing effects. This was also seen when the continuum limit of the quenched theory was taken [25]. Other QNS, including those shown in Fig. 2, are reasonably close to their continuum weak-coupling limit already for $N_t = 8$.

In Fig. 4 we show two different series of susceptibilities. The first panel shows diagonal QNS, χ_{n0}. A little below T_c their magnitudes rise very rapidly with the order. A little above T_c the higher order QNS also approach their weak-coupling values. χ_{40} peaks near T_c, and then approaches a nonvanishing ideal-gas value for large T. $\chi_{60}T^2$ also seems to peak around the same temperature, but it approaches zero above T_c. In the second part of this figure we show the BNS. Their magnitudes also rise very fast with order just below T_c. While the second order QNS vary monotonically with temperature, the fourth and sixth orders peak around T_c [4]. Since these QNS are measured using the same gauge configurations and fermion source vectors, their errors are strongly correlated. This cannot be shown in the figure, but is important for the error estimation in all the succeeding analysis. Our bootstrap process is designed to take care of these covariances.

By comparing the coefficients of any two terms in the Maclaurin series for χ_B induced by the expansion given in Eq. (1), we have estimators of the radius of convergence

$$\mu_B^{m/n} = \left[\frac{(n-2)!\chi_B^m}{(m-2)!\chi_B^n}\right]^{1/(n-m)}. \tag{4}$$

The radius of convergence generally corresponds to a singularity at complex μ. However, when all the χ^n are positive, then this singularity lies on the real axis. In a bootstrap analysis, one requires this criterion for all samples, since the mean would have an imaginary part otherwise. We find that this selects out $\beta = 5.50$, which

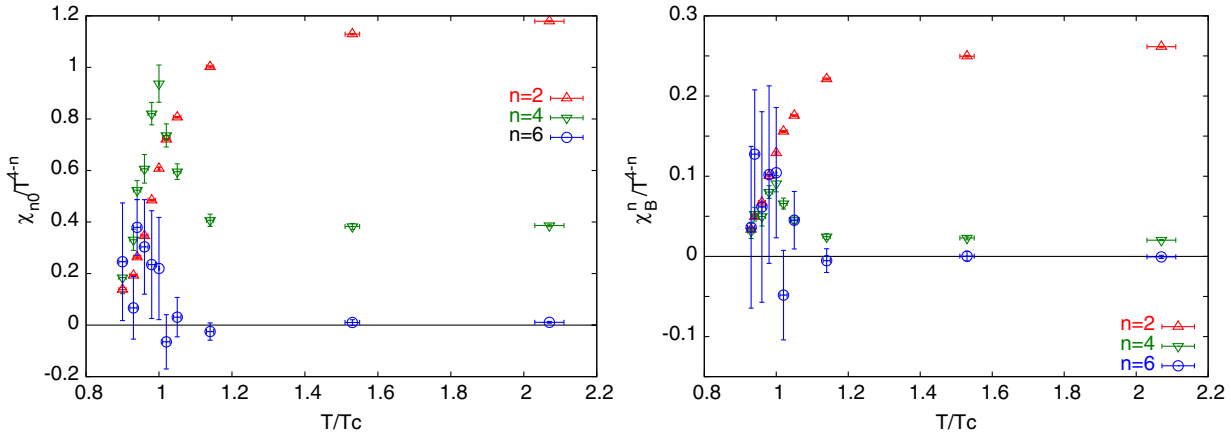

FIG. 4. Measurements of various susceptibilities for $N_t = 8$. The diagonal QNS χ_{20}/T^2 (up triangles), $\chi_{40}/2$ (down triangle) and $T^2\chi_{60}/24$ (circles) are shown in the first panel. In the second panel we show the baryon number susceptibilities, χ_B^2/T^2 (up triangles), χ_B^4 (down triangles) and $T^2\chi_B^6$ (circles).

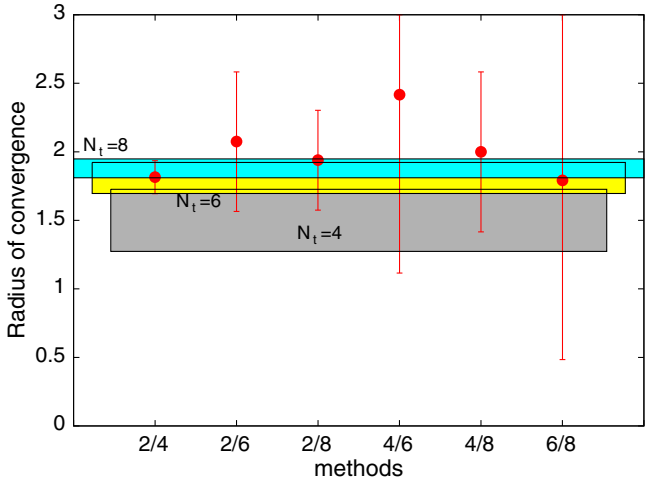

FIG. 5. Estimating the radius of convergence of the series at the temperature where it is found to be real. All the different estimators $\mu_B^{m/n}$ are shown (circles) along with the bootstrap estimator of their mean (the band marked $N_t = 8$). Also shown are the bands of estimates obtained in previous computations.

corresponds to a temperature of $0.94T_c$. In each bootstrap sample one obtains all possible $\mu_B^{m/n}$. These bootstrap estimators are shown in Fig. 5. In each bootstrap sample one may take an average over all the estimators. The figure also shows the bootstrap estimator of the average, drawn as the band labeled $N_t = 8$. This gives the location of the critical point of QCD as

$$\frac{\mu_B^E}{T^E} = 1.85 \pm 0.04, \quad \text{and} \quad \frac{T^E}{T_c} = 0.94 \pm 0.01. \tag{5}$$

This should be compared with the estimated $\mu_B^E/T^E = 1.8 \pm 0.1$ for $N_t = 6$ [8] and the recent high-statistics determination $\mu_B^E/T^E = 1.5 \pm 0.2$ for $N_t = 4$ [4], which are also shown as bands labeled by N_t in Fig. 5. Note again that our convention is to choose T_c to be the temperature at which the Polyakov loop susceptibility peaks. The continuum value for this quantity was reported in [26].

A recent computation in $2+1$ flavor QCD with an imaginary chemical potential finds a lack of evidence for a critical point after analytic continuation to real chemical potential [27]. Since the phase diagram in imaginary chemical potential is very different, it is not yet clear what effect this has on the analytic continuation. Further comparison of computations with real and imaginary chemical potential will be useful and interesting.

IV. CRITICAL BEHAVIOR AND EQUATION OF STATE

Having determined the BNS, *i.e.*, the Maclaurin series coefficients of ΔP and n, one can use these to determine the EOS at finite z through a truncated series expansion. This must be a reasonable approximation to use when one needs the EOS at small μ_B. However, how small these μ_B should be is a question which must be determined using the series itself. Clearly, in the temperature range close to our estimated T^E a truncated series expansion fails badly, because each of the neglected terms could be as large as the terms included. In this case one needs to resum the series. After this is done one can quantitatively estimate the range of μ_B where the truncated series is useful.

A power divergence in χ_B, as in Eq. (2), gives a pole in

$$m_1(z,T) = \frac{\partial \log(\chi_B/T^2)}{\partial z} = \frac{\chi_B^3(z,T)/T}{\chi_B^2(z,T)/T^2}. \tag{6}$$

We can convert the series for χ_B/T^2 into a series for m_1. Since this has a simple pole, the series for m_1/z can be approximated by a [0, 1] Padé approximant in z^2. The Padé approximant for m_1 is then of the form $2\psi z/(z_E^2 - z^2)$. This two parameter form resums the series in the whole region of z where the singular form is dominant [4]. $\chi_B^2(z,T)$ is obtained by exponentiating the integral of $m_1(z,T)$ found in this way.

The Padé analysis yields the critical point, *i.e.*, the position of the pole, z_E, as well as the critical exponent ψ [28]. The current statistics is still not good enough to give a sharp estimate of ψ. An interesting point to note is that statistical errors in the series coefficients translate into errors in the location of the pole, thus leading to very large errors in χ_B in the vicinity of z_E. With increasing statistics, this range of z shrinks, as we show in Fig. 6. The growth of the errors as one approaches the radius of convergence is a manifestation of critical slowing down.

If one assumes that the critical exponent is given by the Ising model, *i.e.*, $\psi = 0.79$ [4], then one has a one parameter Padé approximant to the series. This parameter is entirely fixed by one term of the series. The series expansion of the resulting Padé agrees within 68% confidence limits with the

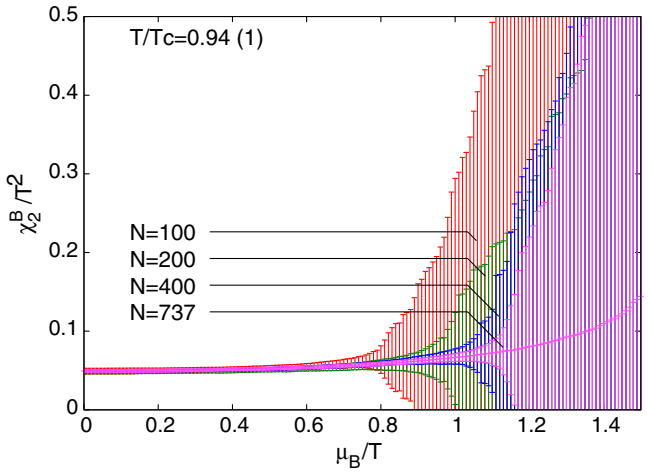

FIG. 6. Critical slowing down manifests itself as the increase in relative error as one extrapolates towards the critical point. As the statistics is increased, this blowup of the error is postponed, but not removed.

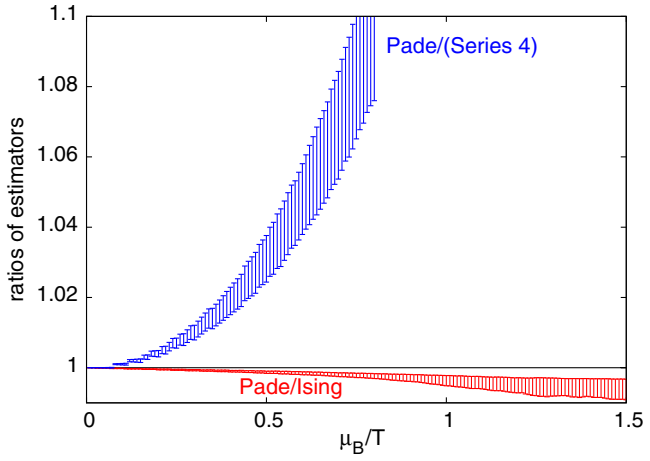

FIG. 7. Comparison of different estimators of $\chi_B^2(z,T)/T^2$ at $T = T_E$. The ratio of the Padé approximant to the series approximation which keeps all BNS up to order 4, called series 4 here, is clearly different from unity, showing that the Padé approximant contains more than two terms of the series. Also shown is the ratio of the Padé approximant to the one with the Ising critical index; this is much closer to unity.

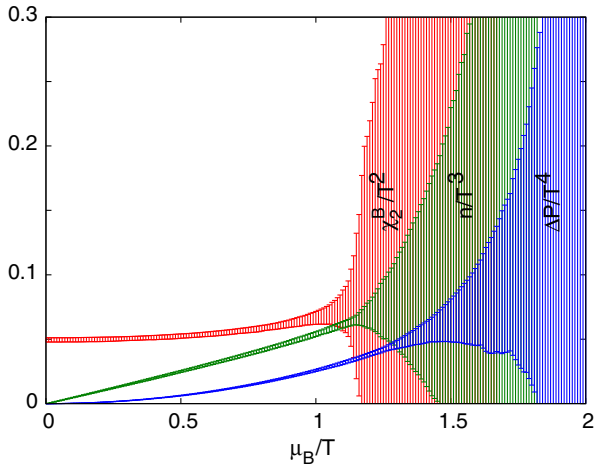

FIG. 8. χ_B/T^2, n/T^3 and $\Delta P/T^4$ for $T/T_c = 0.94(1)$ obtained by successive integration. For the range of $z = \mu_B/T$ over which χ_B/T^2 is constant, the baryon density is linear and the pressure is quadratic. The errors decrease with increasing order of integration because they are not pointwise errors, but induced through the errors in the Padé parameters extracted for m_1.

next terms of the known series. In Fig. 7 we show the ratio of the Padé and the Ising-constrained Padé. They give similar results for $\chi_B^2(T,\mu_B)/T^2$. This implies, of course, that the Ising exponent is compatible with this computation at the 90% confidence level. This computation is also consistent, at the same level, with the mean field value $\psi = 0.66$. In Fig. 7 we also show another ratio. This is the ratio of $\chi_B^2(T,\mu_B)/T^2$ obtained from integrating the Padé approximant of m_1, and that using the truncated series expansion $\chi_B^2(T)/T^2 + \chi_B^4(T)z^2/2$. This truncation is called series (4) in the rest of this paper. A truncation which keeps the z^4 term also is called series (6) later. As one can see from Fig. 7 this ratio is very significantly different from unity, showing that the higher order terms in the full series expansion become more and more important as one approaches the radius of convergence.

The Padé approximant is fitted using two terms of the series expansion of m_1 (one if the Ising critical exponent is taken as an input). If one reexpands the Padé approximant in powers of z, then one has predictions for the infinite series. We verified that the third term of the series for m_1 (coming from the fourth term for χ_B) is consistent with the Padé approximant reexpanded in this way. Similarly we checked for consistency of two terms when the Ising critical exponents is taken as an input.

Using χ_B^2 we can make an estimate of the width of the critical region. This is not a very well-defined concept, but is usually taken as an estimate of the region in which the regular part of the free energy is negligible compared to the singular part. We convert this to a numerical estimate by asking at which value of z does χ_B become 5 times its value at $T = T^E$ and $z = 0$. By this criterion one enters the critical region when $\mu_B = 1.6T^E$, *i.e.*, at $\mu_B = 0.87\mu_B^E$. If one asks the more stringent question, when does χ_B become 10 times its value, then we find that the critical region begins when $\mu_B = 0.96\mu_B^E$. These estimates use mean values. As one can see in Fig. 8, the uncertainties on these estimates are currently very large.

From this description of χ_B one obtains the EOS, namely n and ΔP, by successive integrations. This is shown in Fig. 8. Notice that χ_B/T^2 is nearly constant until $z \simeq 0.5$, as a result of which n is close to linear and ΔP is almost quadratic. Note also that the range of critical slowing down is smaller with increasing number of integrations. The reason for this is simply that the errors shown in the figures are not pointwise errors in z, but are induced by an error in z_E. With increasing number of integrations, the singularity at z_E becomes milder, as a result of which the errors also become easier to control.

It is interesting that this analysis is also a good numerical description of the data at $T/T_c \simeq 2$. There the terms of the series expansion beyond the fourth order are statistically insignificant. The Padé resummation deals with this by pushing the pole out to very large z. At such temperatures we see that the truncated series and the Padé approximant gives similar results.

Our main results for the EOS are shown in Fig. 9. We display n, ΔP, and the isothermal bulk compressibility, κ, as a function of μ_B/T at several fixed temperatures below T_c, as well as a function of T/T_c for several different values of μ_B/T. As before, there are two regimes of temperature: above and below T_c. In the region $T > T_c$, the EOS is dominated by the two QNS χ_{20} and χ_{40} which are non-vanishing even in the ideal gas. These have strong lattice spacing dependence, leading to large cutoff dependence in the absolute value of the EOS in this high temperature

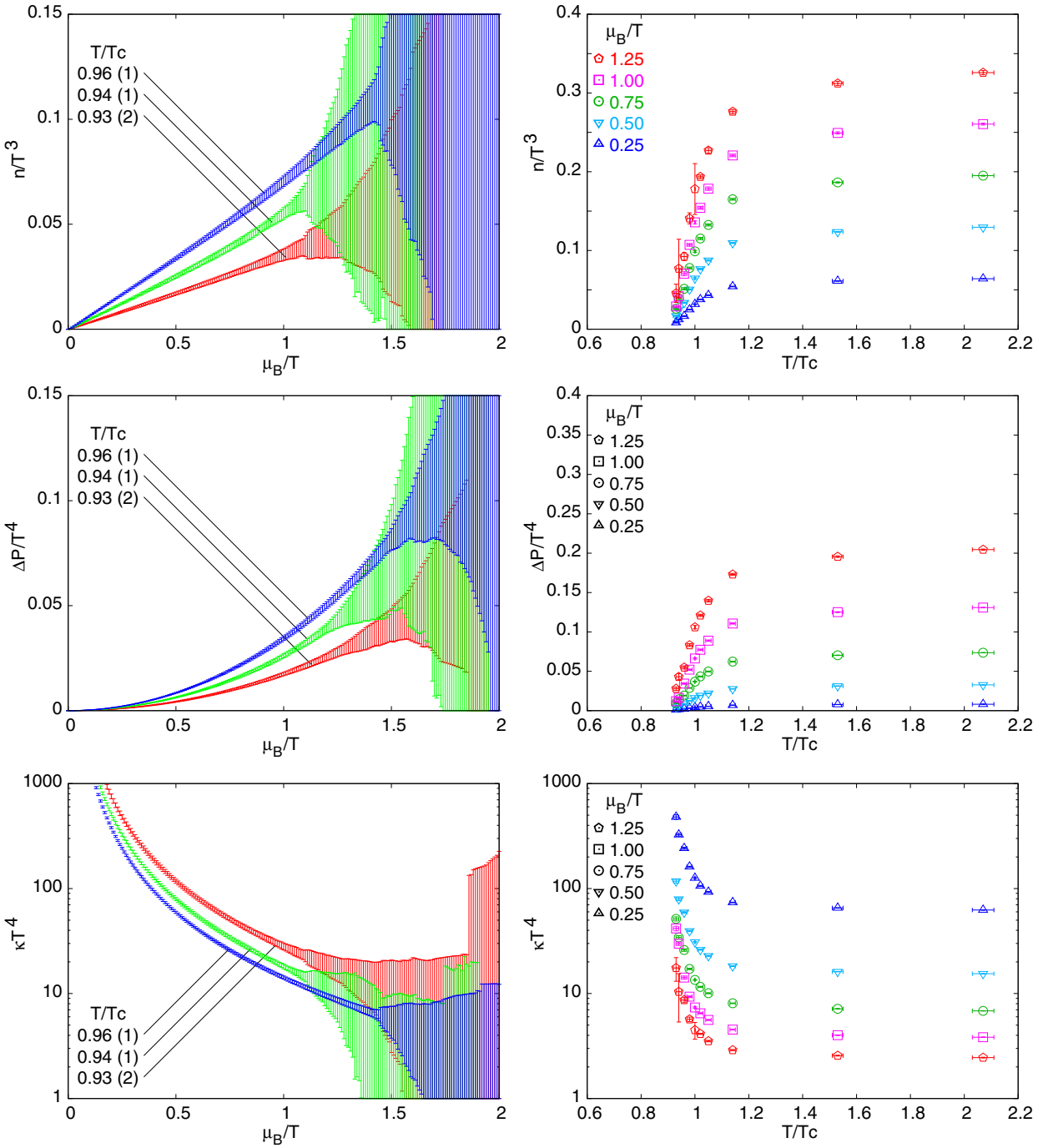

FIG. 9. The equation of state, $n(\mu_B, T)/T^3$ and $\Delta P(\mu_B, T)/T^4$, and the isothermal bulk compressibility, $T^4\kappa(\mu_B, T)$. These are insensitive to the lattice spacing for $T < T_c$.

region [29]. However, a comparison with the results of [4] show that for $T < T_c$ the EOS is beginning to stabilize even for μ_B/T as large as 1.5.

V. FLUCTUATIONS AND FREEZE-OUT

The study of QNS in lattice QCD has been interesting because of the possibility of contact with experimental data. This may be confounded by the fact that the fluctuations predicted by lattice computations are those in the conserved baryon number, whereas those studied experimentally are in the proton number. The connection between the two have been addressed through hadronic Monte Carlo simulations within event generators and seem to indicate that the comparison is safe. We accept this current understanding in this section, while cautioning the reader that this might

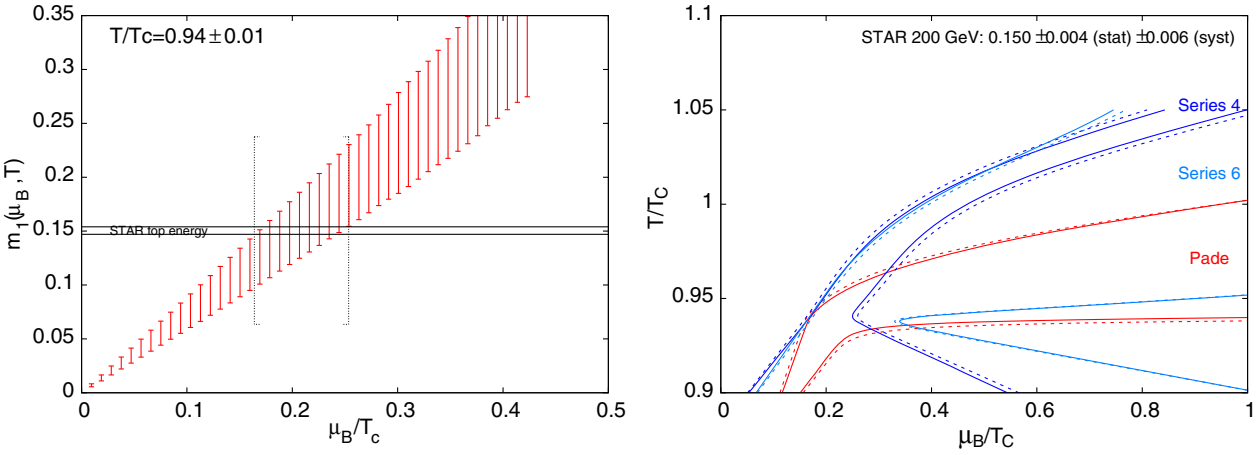

FIG. 10. In the first panel we show a comparison between our determination of m_1^B and the STAR collaboration's measurement for this quantity in the fluctuation of protons at its highest energy. At each T/T_c, such a comparison yields a confidence interval for $z = \mu_B/T$ appropriate for the experimental result. In the second panel we show the smoothed freeze-out band obtained by comparing lattice computations with the STAR data at the highest energy. The band labeled "series 4" is obtained with the Taylor series including the fourth order BNS, "series 6" up to sixth order, "Pade" for the Padé approximant. The dashed line shows the effect of the experimental systematic error on the band.

change as the experimental error bars improve, or the inputs to the event generators are updated.

Measures of fluctuations which have been discussed before [5,16] are

$$m_1^B(\mu_B,T) = \frac{\chi_B^3(\mu_B,T)/T}{\chi_B^2(\mu_B,T)/T^2}, \quad \text{and}$$
$$m_2^B(\mu_B,T) = \frac{\chi_B^4(\mu_B,T)}{\chi_B^2(\mu_B,T)/T^2}, \tag{7}$$

and their ratio $m_3^B = (\chi_B^3/T)/\chi_B^4$. The quantity

$$m_0^B = \frac{n(\mu_B,T)}{\chi_B^2(\mu_B,T)} \tag{8}$$

has also been proposed, as have various other combinations of these ratios [32]. Such ratios can also be defined for charge fluctuations. The ansatz of Eq. 2 has been used to investigate the ratios in Eq. (7). Predictions for these observables in colliders have also been made using the track of the freeze-out points across the phase diagram as one changes $\sqrt{S}$, the center of mass energy of the collider [5]. First comparisons of lattice computations with experimental results have successfully given rise to new ways of approaching questions such as the physical value of T_c [17], or conversely, the freeze-out conditions [18].

We have discussed the computation of m_1^B in detail in the previous section. Here we follow a program outlined in [5,16] to discuss a detailed comparison with data from [7], in order to find the point on the phase diagram where the fluctuations freeze out. The extrapolation of m_1 in μ_B/T for each temperature can be compared with the data to find possible range of chemical potentials allowed by the data. We show an example in the first panel of Fig. 10 where the Padé approximant to m_1^B obtained at $T/T_c = 0.94 \pm 0.01$ is compared to the data from the STAR experiment at $\sqrt{S} =$ 200 GeV [7]. One can see that the error in the freeze-out chemical potential is dominated by the statistical error in the lattice computation. The analysis shown in this panel of the figure is naive, since it compares the 68% probability bands of the experiment with the lattice computation. We improve this estimate by putting such a comparison within a bootstrap and extracting the 68% confidence limits on the fit using the bootstrap distribution of this estimate. We find that this shifts the band marginally compared to the naive estimate. In the same way, truncated series for m_1 can be used to determine freeze-out parameters.

One datum cannot determine both the parameters μ_B and T, so this comparison gives us a strip of allowed values in the phase diagram, as shown in the second panel of Fig. 10. We have used Bernstein polynomials for smoothing. The figure shows differences between a truncated power series and the Padé approximant. Also the truncated power series taken to different orders yields bands which are somewhat different. Previous computations [18] have used a truncated power series taken to the fourth order. We argued before that this misses potentially large contributions from higher order computations. In the figure we also show the contribution when the power series includes the sixth order BNS, and when the Padé resummation of the series is performed. In the difference between the fourth and sixth order series expansions, the systematic errors from the truncation of the series are mixed with statistical errors in the determination of the coefficients. The Padé approximant is an attempt to remove the systematic errors due to

series truncation. We expect that further improvements in computation will shrink the error bands.

The further condition that freeze-out occurs at the chiral crossover is imposed in [18]. At this temperature [33], the truncated series method gives a freeze-out value for μ_B which roughly matches that found from a phenomenological analysis of hadron yields [14]. However, our analysis shows that there are significantly larger theory uncertainties. Improvements in the statistical errors in lattice computations will have many consequences for the late-stage physics of heavy-ion collisions, including shedding light on the very mechanism of freeze-out.

VI. CONCLUSIONS

In this paper we reported measurements of the QNS in QCD at finite temperature with two flavors of light staggered quarks using lattices with temporal extents of $N_t = 8$. We have determined the $\mu_B = 0$ crossover coupling $\beta_c = 5.53$ using the peak in the Polyakov loop susceptibility. In Sec. II we presented the evidence that different numbers of source vector are required to obtain reliable measurements of QNS at different orders. For the second order QNS a hundred vectors is sufficient, but at least 1000 fermion source vectors are needed to get good measurements for QNS of order 6 for $T < T_c$ whereas substantially smaller number of source vectors are required in the high temperature phase (see Fig. 1). We have used 2000 source vectors at each temperature below T_c and 800 or 1600 source vectors above T_c in this study.

We compared measurements of the off diagonal QNS χ_{11}/T^2 made with different lattice spacings in Fig. 3. This comparison indicates that the $N_t = 8$ results for this QNS may be close to the continuum limit. The diagonal QNS χ_{20}/T^2 is also shown in this figure. Above T_c there is clear evidence of finite lattice spacing effects in χ_{20}/T^2. The reason for this is interesting. A particular operator which contributes only to χ_{20}/T^2 has large lattice spacing effects for free staggered quarks. All other QNS are close to the continuum limit predicted by weak-coupling theory, as shown in Fig. 2. In the temperature range below T_c there is good agreement between earlier results for χ_{20}/T^2 for $N_t = 6$ [8] and the new results. This indicates that in the confined state these results may be close to the continuum limit.

We have also shown our measurements of several of the higher order QNS in Fig. 4. There is structure visible in these QNS in the neighborhood of T_c. The fact that these measurements are made using the same configurations and source vectors makes them strongly correlated with each other, something that the error bars shown in the figures cannot capture. This has consequences for all derived measurements.

At $T/T_c = 0.94 \pm 0.01$ we find the radius of convergence of the Taylor series expansion for the BNS is $\mu/T = 1.85 \pm 0.04$ (see Fig. 5). At this temperature all the terms in the series which we can measure turn out to be positive, implying that the singular point is on the real axis. This leads us to believe that the radius of convergence identifies a critical point of QCD. We note that this estimate is completely consistent with that presented earlier for $N_t = 6$ in [8].

The existence of a finite radius of convergence of a series expansion is a statement of the mathematical fact that the successive terms of the series become equal at the radius of convergence. This means that in deriving consequences from the series, one cannot afford to truncate the series, but must attempt to sum all the terms. A method of doing this through Padé approximants was first used in [4] with lattice spacing which is about twice of what we use here. This also gives an independent, though coarse, check on the estimate of the radius of convergence referred to earlier. We have used the same method in Sec. IV to continue the equation of state to finite chemical potential. Our results for the baryon number density, $n(\mu_B, T)/T^3$, as a function of temperature and chemical potential, the change in the pressure due to the chemical potential, $\Delta P(\mu_B, T)/T^4$, and the isothermal bulk compressibility, $T^4\kappa$, are shown in Fig. 9.

It is known that direct Monte Carlo simulations suffer from critical slowing down, due to the unbounded growth of correlations near a critical point. A similar phenomenon is observed in the reconstruction of physical quantities using series expansions, as demonstrated in Fig. 6. In spite of this, we are able to extract the equation of state up to $\mu_B/T \simeq 1.25$ with reasonable accuracy.

In Sec. V we examine the influence of the full series expansion in connecting to data on fluctuations. We show that truncating the series expansion [18] leads to changes in the determination of the freeze-out conditions for fluctuations. This includes statistical and systematic theory uncertainties. We have shown, in the right-hand panel of Fig. 10, that the results shift when truncating the series expansion up to the fourth order BNS or the sixth order. We have also shown the results obtained when we try to estimate the complete series by a Padé resummation. These uncertainties can be bounded better in future by going to larger orders in the series expansion. The full analysis which was suggested in [5] is needed to make contact with experimental data. This is, of course, equally true for the equation of state.

We have examined a previously underappreciated source of systematic errors in the reconstruction of physical quantities from Taylor series expansions, namely the truncation errors in the series expansion. While our measurements are restricted to moderate lattice spacings, *i.e.*, $1/(8T)$, we have presented some evidence that the systematic errors arising from extrapolations in lattice spacing are much smaller than these truncation errors. Future work will concentrate on reducing statistical and both kinds of systematic errors.

ACKNOWLEDGMENTS

The computations described here were carried out on the IBM BlueGene P of the ILGTI in TIFR. We thank Ajay Salve and Kapil Ghaliadi for technical support. We would like to thank Alexi Vuorinen and Sylvain Mogliacci for sharing code and tables of their weak coupling computations.

[1] S. Gottlieb, W. Liu, D. Toussaint, R. L. Renken, and R. L. Sugar, Phys. Rev. Lett. **59**, 2247 (1987).
[2] R. V. Gavai and S. Gupta, Phys. Rev. D **68**, 034506 (2003).
[3] R. V. Gavai and S. Gupta, Phys. Rev. D **71**, 114014 (2005).
[4] S. Gupta, N. Karthik, and P. Majumdar, Phys. Rev. D **90**, 034001 (2014).
[5] R. V. Gavai and S. Gupta, Phys. Lett. B **696**, 459 (2011).
[6] M. M. Aggarwal *et al.* (STAR Collaboration), Phys. Rev. Lett. **105**, 022302 (2010).
[7] L. Adamczyk (STAR Collaboration), Phys. Rev. Lett. **112**, 032302 (2014).
[8] R. V. Gavai and S. Gupta, Phys. Rev. D **78**, 114503 (2008).
[9] S. Datta, R. V. Gavai, and S. Gupta, Nucl. Phys. A **904–905**, 883 (2013).
[10] S. Datta, R. V. Gavai, and S. Gupta, *Proc. Sci.*, LAT2013 (2013) 202.
[11] R. V. Gavai and S. Gupta, Phys. Rev. D **73**, 014004 (2006).
[12] M. Cristoforetti, T. Hell, B. Klein, and W. Weise, Phys. Rev. D **81**, 114017 (2010); A. Bhattacharyya, P. Deb, A. Lahiri, and R. Ray, Phys. Rev. D **82**, 114028 (2010).
[13] T. K. Herbst, J. M. Pawlowski, and B. J. Schaefer, Phys. Rev. D **88**, 014007 (2013).
[14] J. Cleymans, H. Oeschler, and K. Redlich, Phys. Rev. C **59**, 1663 (1999); A. Andronic, P. Braun-Munzinger, and J. Stachel, Nucl. Phys. **A772**, 167 (2006); F. Becattini, J. Manninen, and M. Gazdzicki, Phys. Rev. C **73**, 044905 (2006); S. Chatterjee, R. M. Godbole, and S. Gupta, Phys. Lett. B **727**, 554 (2013); K. A. Bugaev, D. R. Oliinychenko, J. Cleymans, A. I. Ivanytskyi, I. N. Mishustin, E. G. Nikonov, and V. V. Sagun, Europhys. Lett. **104**, 22002 (2013); F. Becattini, J. Steinheimer, R. Stock, and M. Bleicher, Phys. Lett. B **764**, 241 (2017).
[15] V. Koch, A. Majumder, and J. Randrup, Phys. Rev. Lett. **95**, 182301 (2005).
[16] S. Gupta, *Proc. Sci.*, CPOD2009 (2009) 025.
[17] S. Gupta, X.-F. Luo, B. Mohanty, H.-G. Ritter, and N. Xu, Science **332**, 1525 (2011).
[18] A. Bazavov *et al.*, Phys. Rev. Lett. **109**, 192302 (2012); S. Borsanyi, Z. Fodor, S. D. Katz, S. Krieg, C. Ratti, and K. K. Szabo, Phys. Rev. Lett. **111**, 062005 (2013).
[19] R. D. Pisarski and F. Wilczek, Phys. Rev. D **29**, 338 (1984).
[20] Y. Aoki, G. Endrodi, Z. Fodor, S. D. Katz, and K. K. Szabo, Nature (London) **443**, 675 (2006).
[21] Y. Aoki, S. Borsanyi, S. Durr, Z. Fodor, S. D. Katz, S. Krieg, and K. K. Szabo, J. High Energy Phys. 06 (2009) 088.
[22] S. Gottlieb, A. Krasnitz, U. M. Heller, A. D. Kennedy, J. B. Kogut, R. L. Renken, D. K. Sinclair, R. L. Sugar, D. Toussaint, and K. C. Wang, Phys. Rev. D **47**, 3619 (1993).
[23] S. Datta and S. Gupta, Phys. Rev. D **80**, 114504 (2009).
[24] S. Mogliacci, J. O. Andersen, M. Strickland, N. Su, and A. Vuorinen, J. High Energy Phys. 12 (2013) 055.
[25] R. V. Gavai and S. Gupta, Phys. Rev. D **67**, 034501 (2003).
[26] Y. Aoki, Z. Fodor, S. D. Katz, and K. K. Szabo, Phys. Lett. B **643**, 46 (2006).
[27] M. D'Elia, G. Gagliardi, and F. Sanfilippo, arXiv: 1611.08285.
[28] With better statistics we should be able to see the small difference between the z_E defined in this way and through Eq. (4).
[29] Usually improved fermion actions are used to alleviate this problem. However, experience has shown that continuum extrapolation remains important even so [30,31]. This improvement comes at a large cost in CPU time.
[30] R. V. Gavai and S. Gupta, Phys. Rev. D **67**, 034501 (2003).
[31] A. Bazavov *et al.*, Phys. Rev. D **85**, 054503 (2012); A. Bazavov *et al.* (HotQCD Collaboration), Phys. Rev. D **90**, 094503 (2014).
[32] C. Athanasiou, K. Rajagopal, and M. Stephanov, Phys. Rev. D **82**, 074008 (2010).
[33] Due to the difference in conventions used to define T_c, in our convention this implies that $T/T_c \simeq 0.94$.